Double Beta Decay of ^{48}Ca

A. Balysh,[1] A. De Silva,[2] V. I. Lebedev,[1] K. Lou,[3] M. K. Moe,[2] M. A. Nelson,[2] A. Piepke,[3] A. Pronskiy,[1] M. A. Vient,[2] and P. Vogel[3]

[1]*Kurchatov Institute, Kurchatov Square, 123182 Moscow, Russia*
[2]*Department of Physics and Astronomy, University of California Irvine, Irvine, California 92697*
[3]*Physics Department, California Institute of Technology, Pasadena, California 91125*

(Received 2 August 1996)

^{48}Ca, the lightest experimentally accessible double beta decay candidate, is the only one simple enough to be treated exactly in the nuclear shell model. Thus the $\beta\beta_{2\nu}$ half-life measurement, reported here, provides a unique test of the nuclear physics involved in the $\beta\beta$ matrix element calculation. Enriched ^{48}Ca sources of two different thicknesses have been exposed in a time projection chamber. We observe a half-life of $T^{2\nu}_{1/2} = (4.3^{+2.4}_{-1.1}[\mathrm{stat}] \pm 1.4[\mathrm{syst}]) \times 10^{19}$ yr, consistent with shell model calculations. [S0031-9007(96)01989-8]

PACS numbers: 23.40.Hc, 21.10.Tg, 21.60.Cs, 27.40.+z

Neutrinoless double beta decay ($\beta\beta_{0\nu}$) is the most sensitive known test for Majorana neutrino mass. The unfolding of a mass value (or limit) from measured decay rates relies on complicated nuclear structure calculations [1]. Comparison of theoretical and experimental rates for the standard $\beta\beta_{2\nu}$ mode is an important test for the validity of these calculations.

Among all realistically measurable candidates for $\beta\beta$ decay, $^{48}\mathrm{Ca} \rightarrow {}^{48}\mathrm{Ti}$ is unique since it is the only one which can be treated "exactly" in the nuclear shell model by solving the problem of eight nucleons distributed within the fp shell without truncation. Consequently, this decay has been a favored testing ground of nuclear theories [2]. However, until now only a lower limit of the $\beta\beta_{2\nu}$ decay half-life, $T^{2\nu}_{1/2} > 3.6 \times 10^{19}$ yr, has been determined experimentally [3].

The nuclear shell model, constrained by the requirement that it describe well the spectroscopy of the $A = 48$ nuclei, restricts the corresponding half-life also from above, $T^{2\nu}_{1/2} \leq 10^{20}$ yr [4]. Therefore the experimental observation of the decay acquires added significance; if it turns out that the shell model cannot predict this theoretically tractable rate, we have to wonder about our ability to describe the nuclear matrix elements in the more complex nuclei. Here we present the result from a new experiment using a time projection chamber (TPC).

The search for $\beta\beta$ decay of ^{48}Ca was among the first to be attempted in live-time experiments beginning in the early fifties (for an extensive chronology see [1]). With the largest energy release of all $\beta\beta$ candidates, ^{48}Ca ($Q_{\beta\beta} = 4.271 \pm 0.004$ MeV [5]) has a $\beta\beta_{2\nu}$ sum-energy spectrum that extends to higher energies than most radioactive backgrounds. Yet calcium has a tendency to harbor chemically similar radio-impurities such as ^{90}Sr and ^{226}Ra, which do intrude on a major fraction of the ^{48}Ca spectral range.

When the two β particles are tracked in a TPC they are seen to both carry negative charge, originate from a common point, and have separately measured energies. Although this distinctive visualization eliminates the bulk of unrelated activity, there remain several well-known mechanisms for production of negative electron pairs that constitute background for $\beta\beta$ decay. The most serious of these are Möller scattering of single β particles and β-γ cascades in which a γ ray internally converts or Compton scatters. These processes are fed principally by the primordial decay chains, but also by cosmogenic and man-made radionuclides. Decay-chain induced background events can often be tagged by α or β particles from neighboring links if the source is thin enough to allow the tagging particles escape into the TPC gas.

The miniscule 0.187% natural abundance of ^{48}Ca makes enrichment both necessary and expensive. Potential loss of costly isotope is a deterrent to chemical purification or conversion to the lightest stable compound. The material used was supplied by the Kurchatov Institute as finely powdered $CaCO_3$ enriched to 73% in ^{48}Ca, and relatively free of U and Th (<0.8 ppb by mass spectroscopic analysis). The $CaCO_3$ powder was injected into a large glass box in bursts of compressed Ar, allowed to settle uniformly onto a 4 μm Mylar substrate, then fixed with a mist of Formvar. Two such deposits, face-to-face, formed the first $\beta\beta$ source, with a total of 42.2 g of $CaCO_3$ (18.5 mg/cm^2 total thickness with substrate and binder).

The shielded UC Irvine TPC [6,7] containing the $\beta\beta$ source as the central electrode in a magnetic field was located in a tunnel at the Hoover Dam under a minimum of 72 m of rock. Data were recorded on magnetic tape, and subsequently passed through stripping software to select clean $1e^-$ and $2e^-$ events. The $2e^-$ events were individually scanned. All unambiguous negative pairs emitted from opposite sides of the source with a common point of origin were fitted with helices, and the parameters written to a $\beta\beta$ candidate file or a ^{214}Bi file, depending on whether a ^{214}Po α particle appeared at the vertex within the following millisecond. The far more numerous $1e^-$ events were fitted automatically by software and also written to a parameter file.

The lone electron ($1e^-$) spectrum plotted against kinetic energy (K) in Fig. 1 represents the total beta activity of source contaminants, and can be broken down into the contributions from individual radionuclides by a least squares fit. ^{90}Sr (2250 μBq/g), ^{226}Ra (530 μBq/g), and their daughters account for the bulk of the spectrum. Contributions from ^{137}Cs (940 μBq/g) and daughters of ^{228}Ra (90 μBq/g) are also present. The two Ra activities, being much larger than the mass spectroscopic limits on U and Th, indicate severe breaking of equilibrium in the respective series. Single β decay of ^{48}Ca is allowed, with a half-life in excess of 6×10^{18} yr [8] corresponding to a specific activity of less than 15 μBq/g. Any background from β decay of ^{48}Ca or its daughter ^{48}Sc through the above-mentioned processes is insignificant. The daughters of greatest concern ($Q_\beta > 2$ MeV) are ^{90}Y, ^{214}Bi, ^{228}Ac, ^{212}Bi, and ^{208}Tl. As a check of the fitting procedure, the energy spectrum of electrons tagged by ^{214}Po α particles was noted to closely match the fitted ^{214}Bi component when adjusted for the α escape probability ($P_\alpha = 0.24 \pm 0.01$ from an independent measurement).

The activities determined from the lone electron spectrum were used as input to a Monte Carlo calculation of the $2e^-$ background. ^{90}Sr and its daughter ^{90}Y are essentially pure β emitters and contribute only through Möller scattering. The other high Q_β nuclei have complex decay schemes with multiple gamma rays [9], all of which were included in the Monte Carlo with their corresponding conversion coefficients. Most of these simulated $2e^-$ backgrounds were directly testable against TPC measurements, with good agreement: The measured ^{214}Bi component was simply the $2e^-$ data subset tagged by the ^{214}Po α and corrected for the α escape probability. The ^{90}Y $2e^-$ measurement was provided by a drop of ^{90}Sr solution applied to a natural isotopic replica of the ^{48}Ca source and placed in the TPC. The ^{212}Bi and ^{208}Tl $2e^-$ measurements were scaled from those produced after an injection of ^{220}Rn, by comparing observed rates of the rapid ^{212}Bi-^{212}Po, β-α sequence.

Since the Monte Carlo $2e^-$ rates were derived from intrinsic activity levels in μBq/g, their agreement with direct measurements also confirms the Monte Carlo predicted $2e^-$ efficiency of the TPC. A Monte Carlo generated background spectrum was essential only for ^{228}Ac where we have no TPC measurement, but in our $2e^-$ background model we elected to use the smoother, better-statistics Monte Carlo spectra for the other contributions as well.

An alternative determination of $2e^-$ background was carried out by a separate subgroup of the collaboration and included independent Monte Carlo calculations and a greater reliance on the above-mentioned TPC measurements as opposed to lone-electron fits. We refer to this direct measurement method as analysis "A," and the lone-electron based method as analysis "B." To eliminate events with the poorest energy resolution, analysis B included a cut on electrons making the smallest angles with the magnetic field ($|\cos(\theta)| < 0.9$).

The $2e^-$ sum spectrum from the ^{48}Ca source, after event-by-event removal of the α-tagged ^{214}Bi, is shown in Fig. 2(a) with a singles threshold of 400 keV. The various remaining background spectra as determined by analysis A are superimposed. The residual spectrum following background subtraction appears in Fig. 2(b). Comparison of the residual spectrum with the theoretical $\beta\beta$ shape results in a $\chi^2/DF = 0.9$ (analysis interval 0.8–3.2 MeV).

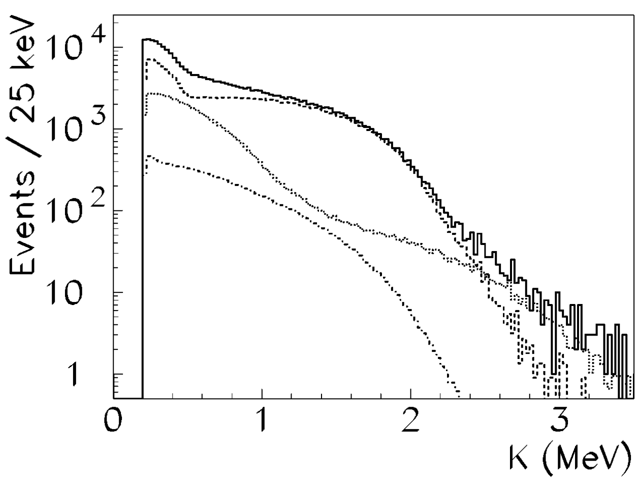

FIG. 1. The lone electron spectrum for the thick source, and the most important of the fitted components. From top to bottom at low energy are the total spectrum, ^{90}Sr, ^{226}Ra, and ^{228}Ra. Daughters are assumed in equilibrium, with the exception of ^{210}Pb. Its daughter ^{210}Bi was fitted separately, then included in the ^{226}Ra curve.

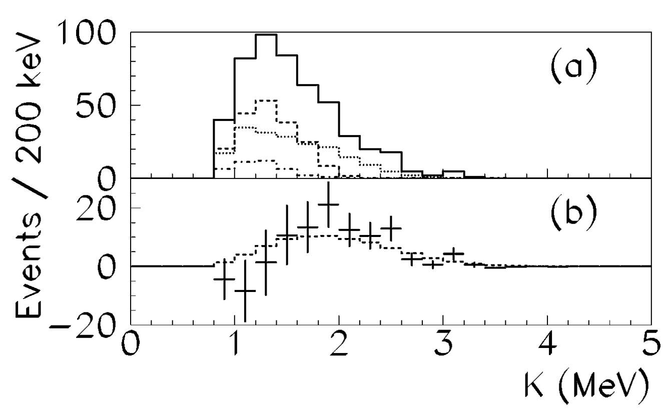

FIG. 2. (a) The measured $2e^-$ sum-energy spectrum and background spectra for the thick source with a 400 keV singles threshold. From top to bottom at low energy are the total measured spectrum, Möller events, ^{214}Bi, and daughters of ^{228}Ra. (b) Residual $\beta\beta$ candidates and Monte Carlo Primakoff-Rosen $\beta\beta$ spectrum at the corresponding $T_{1/2}^{2\nu} = 4.1 \times 10^{19}$ yr obtained at this threshold (dashed line).

The above procedure was repeated for a series of singles thresholds and one relatively high sum threshold, with consistent results. The corresponding half-lives were calculated in each case, as shown for two of the threshold combinations in Table I. The 2 MeV sum threshold was accompanied by an additional singles spectrum cut on the strong ^{214}Bi conversion line at 1.3 MeV. Quoted errors in the table are statistical. The calculated half-life is independent of threshold and of analysis A or B within errors.

Since the half-life precision was degraded by the unexpectedly large Ra and Sr contamination, the 42.2 g source was replaced after 2440 hours exposure with one containing only 10.3 g of enriched $CaCO_3$ and total thickness 5.4 mg/cm^2. The thinner source was exposed 4001 hours, and these results are also included in Table I. The ^{214}Bi rejection improved greatly as a result of an increase in P_α from 0.24 to 0.69, and the ^{90}Y component was weakened by the large reduction in target mass for Möller scattering. The thin-source analog of Fig. 2(b) yields $\chi^2/DF = 1.0$. It is encouraging that despite different dependence on source mass for the ^{48}Ca signal and the background rates (particularly ^{214}Bi) the half-lives derived from thick and thin sources agree within statistics.

The thick and thin source residual spectra were each corrected for energy loss and efficiency distortion, then combined for the Kurie plot shown in Fig. 3(a). Including the singles threshold (ϵ) and using the Primakoff-Rosen approximation [10] for the Coulomb effect leads to the Kurie plot formula

$$((dN/dK)/\{(K-2\epsilon)[f_0(K)+f_\epsilon(K)]\})^{1/5} \propto (Q_{\beta\beta}-K)\,;$$

$$f_0(K) = K^4/30 + K^3m/3 + 4K^2m^2/3 + 2Km^3 + m^4,$$

$$f_\epsilon(K) = \epsilon(K-\epsilon)[K^2/15 + 2Km/3 + 2m^2/3 + \epsilon(K-\epsilon)/5],$$

with electron mass (m) and the sum kinetic energy (K). (The approximation produces <1% distortion over the plotted range.) The Kurie plot energy intercept at 4.2 ± 0.1 MeV is consistent with the ^{48}Ca $Q_{\beta\beta}$ value of 4.27 MeV. The small error bars resulting from the Kurie transformation have been omitted in the figure. By comparison, in Fig. 3(b) the α-tagged ^{214}Bi $2e^-$ events produce an intercept of 3.8 ± 0.1 MeV, and in Fig. 3(c) the plot for measured ^{208}Tl ($Q_\beta = 5.0$ MeV) events is grossly nonlinear.

Since the thick and thin sources were exposed separately, corresponding pairs of columns in the table can be combined as independent measurements. For example, combining thick and thin $\beta\beta$ events for 0.400/0.800 MeV singles/sum thresholds, analysis A, yields $T_{1/2}^{2\nu} = (4.3^{+2.4}_{-1.1}) \times 10^{19}$ yr. Either of the other two thick-thin pairs would combine to give an equally valid result. However, since the other two results would

TABLE I. Breakdown of counts from the two sources for two energy thresholds.

	Thick source (0.0775 mol-y)			Thin source (0.0310 mol-y)		
Singles threshold (MeV)	0.400		0.200	0.400		0.200
Sum threshold (MeV)	0.800		2.000	0.800		2.000
^{214}Bi 1.3 MeV line cut	No		Yes	No		Yes
	Analysis A	Analysis B		Analysis A	Analysis B	
Small polar angles cut	No	Yes	No	No	Yes	No
Counts						
With α tag	55	50	6.8 ± 1.4[a]	79	72	8.0 ± 1.6[a]
Without α tag	500	472	72	142	134	21
Backgrounds						
Untagged ^{214}Bi	189.1 ± 25.5	186.3 ± 35.7	23.4 ± 4.9	40.2 ± 4.5	36.4 ± 8.9	4.1 ± 0.8
Möller events[b]	191.5 ± 4.6	163.4 ± 5.6	3.2 ± 0.6	53.7 ± 1.7	46.1 ± 2.1	1.5 ± 0.3
^{228}Ac, ^{212}Bi, ^{208}Tl[c]	42.8 ± 7.5	29.4 ± 5.6	4.0 ± 0.8	19.8 ± 3.5	13.3 ± 2.1	1.4 ± 0.3
Total background	423.3 ± 27.0	379.1 ± 36.6	30.7 ± 5.0	113.7 ± 6.0	95.8 ± 9.4	7.0 ± 0.9
$\beta\beta$ events	76.7 ± 35.0	92.9 ± 42.5	41.3 ± 9.8	28.3 ± 13.3	38.2 ± 14.9	14.0 ± 4.7
Statistical significance	2.2σ	2.2σ	4.2σ	2.1σ	2.6σ	3.0σ
Efficiency[d]	0.097	0.090	0.041	0.105	0.097	0.047
$T_{1/2}^{2\nu}$ (10^{19} y)	$4.1^{+3.5}_{-1.3}$	$3.1^{+2.7}_{-1.0}$	$3.2^{+1.0}_{-0.6}$	$4.8^{+4.2}_{-1.5}$	$3.3^{+2.1}_{-0.9}$	$4.3^{+2.2}_{-1.1}$
Signal/Background	0.18	0.25	1.35	0.25	0.40	2.04
Kurie plot intercept (MeV)	4.1 ± 0.1			4.4 ± 0.1		

[a]Scaled from counts at lower threshold by the ratio observed in a larger ^{214}Bi data set.
[b]Exclusive of ^{214}Bi which is included in the row above.
[c]Exclusive of Möller, which is included in the row above.
[d]From Monte Carlo simulation.

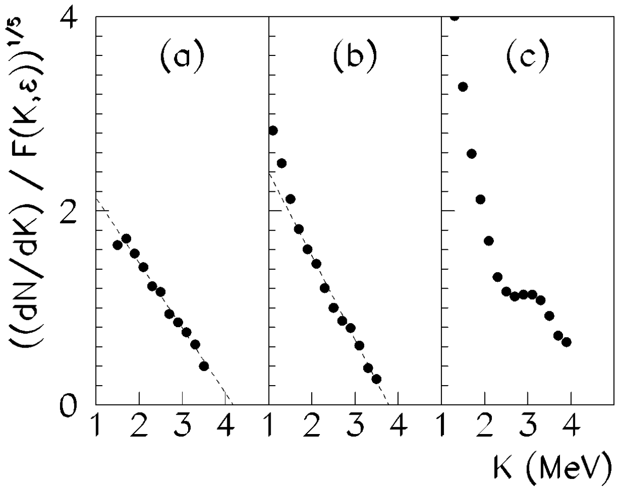

FIG. 3. (a) High-energy portion of the Kurie plot for residual $\beta\beta$ candidates combined from thick and thin sources at a singles threshold of 400 keV. (b) Tagged ^{214}Bi fit over the same range, 1.6–3.6 MeV. (c) ^{208}Tl from ^{220}Rn injection. ($F(K,\epsilon) = (K - 2\epsilon)[f_0(K) + f_\epsilon(K)]$. See text.)

not be statistically independent from the first, we do not attempt a grand average. Rather, we choose the above half-life value for the following reasons. The lower threshold includes a broader range of the spectrum than the 2 MeV sum threshold, and the $2e^-$ TPC background measurements in analysis A are more direct than background levels inferred from the lone-electron spectrum, as in analysis B. We include the A-B analysis difference in the systematic error. The remainder of the systematic error is largely in the detector efficiency. Thus we quote a final result of $T_{1/2}^{2\nu} = (4.3^{+2.4}_{-1.1}[\mathrm{stat}] \pm 1.4[\mathrm{syst}]) \times 10^{19}$ yr. This observation is consistent with the spectroscopy-constrained shell model of Ref. [4].

The high energy threshold cuts (columns 4 and 7 of Table I) contain little spectral shape information. However, we could alternatively select these results because of their high combined statistical significance of 5.0σ. The combined half-life in this case is $T_{1/2}^{2\nu} = (3.5^{+0.9}_{-0.6}[\mathrm{stat}] \pm 0.5[\mathrm{syst}]) \times 10^{19}$ yr, statistically consistent with the low threshold analysis.

Although the ^{48}Ca-enriched sample contained traces of radium and strontium activity, backgrounds were well defined by associated alpha particles and the lone electron spectrum. The residual data give half-life values that are consistent between two $\beta\beta$ sources of different thickness and among various energy thresholds. The corresponding Kurie plots form straight lines which intercept the energy axis near the ^{48}Ca $Q_{\beta\beta}$ value, unlike plots made from measured samples of the various backgrounds. We believe these results constitute strong evidence for ^{48}Ca double beta decay at a half-life supporting the relatively rigid shell model calculations for this light double beta decay nucleus.

We gratefully acknowledge the hospitality of Blaine Hamann and William Sharp at the Hoover Dam. We thank Felix Boehm for his advice and support, and one of us (A. P.) wishes to acknowledge the support of the Alexander von Humboldt Foundation. This work was funded by the U.S. Department of Energy under Contracts No. DE-FG03-01ER40679 and No. DE-FG03-88ER40397.

[1] W. C. Haxton and G. J. Stephenson, Jr., Prog. Part. Nucl. Phys. **12**, 409 (1984).
[2] For a representative list, see F. Boehm and P. Vogel, *Physics of Massive Neutrinos* (Cambridge University Press, Cambridge, England, 1992), 2nd ed.
[3] R. K. Bardin, P. J. Gollon, J. D. Ullman, and C. S. Wu, Nucl. Phys. A **158**, 337 (1970).
[4] A. Poves, R. P. Bahukutumbi, K. H. Langanke, and P. Vogel, Phys. Lett. B **361**, 1 (1995).
[5] A. H. Wapstra and G. Audi, Nucl. Phys. A **432**, 1 (1985).
[6] S. R. Elliott, A. A. Hahn, and M. K. Moe, Nucl. Instrum. Methods Phys. Res., Sect. A **273**, 226 (1988).
[7] M. K. Moe, M. A. Nelson, and M. A. Vient, Prog. Part. Nucl. Phys. **32**, 247 (1994).
[8] D. E. Alburger and J. B. Cumming, Phys. Rev. C **32**, 1358 (1985).
[9] *Table of Isotopes*, edited by C. M. Lederer and V. S. Shirley (John Wiley & Sons, New York, 1978), 7th ed.
[10] H. Primakoff and S. P. Rosen, Rep. Prog. Phys. **22**, 121 (1959).